Biophysical Journal Volume 75 August 1998 745–754

Diffusion and Reaction of Nitric Oxide in Suspension Cell Cultures

Bo Chen, Manish Keshive, and William M. Deen
Department of Chemical Engineering, Massachusetts Institute of Technology, Cambridge, Massachusetts 02139 USA

ABSTRACT A reaction-diffusion model was developed to predict the fate of nitric oxide (NO) released by cells of the immune system. The model was used to analyze data obtained previously using macrophages attached to microcarrier beads suspended in a stirred vessel. Activated macrophages synthesize NO, which is oxidized in the culture medium by molecular oxygen and superoxide (O_2^-, also released by the cells), yielding mainly nitrite (NO_2^-) and nitrate (NO_3^-) as the respective end products. In the analysis the reactor was divided into a "stagnant film" with position-dependent concentrations adjacent to a representative carrier bead and a well-mixed bulk solution. It was found that the concentration of NO was relatively uniform in the film. In contrast, essentially all of the O_2^- was calculated to be consumed within ~2 μm of the cell surfaces, due to its reaction with NO to yield peroxynitrite. The decomposition of peroxynitrite caused its concentration to fall to nearly zero over a distance of ~30 μm from the cells. Although the film regions (which had an effective thickness of 63 μm) comprised just 2% of the reactor volume and were predicted to account for only 6% of the NO_2^- formation under control conditions, they were calculated to be responsible for 99% of the NO_3^- formation. Superoxide dismutase in the medium (at 3.2 μM) was predicted to lower the ratio of NO_3^- to NO_2^- formation rates from near unity to <0.5, in reasonable agreement with the data. The NO_3^-/NO_2^- ratio was predicted to vary exponentially with the ratio of O_2^- to NO release rates from the cells. Recently reported reactions involving CO_2 and bicarbonate were found to have important effects on the concentrations of peroxynitrite and nitrous anhydride, two of the compounds that have been implicated in NO cytotoxicity and mutagenesis.

INTRODUCTION

Nitric oxide (NO) is a biological messenger molecule formed via the oxidation of L-arginine to citrulline by various forms of NO synthase (Marletta, 1993). The synthesis of NO is observed in a wide variety of mammalian cells, including macrophages, vascular endothelial cells, epithelial cells, and neurons. The actions of NO in the body are paradoxical in that it is both a regulatory molecule and an agent which is cytotoxic, mutagenic, and (probably) carcinogenic. Among the important regulatory actions of NO are inhibition of platelet aggregation, vasodilation (blood pressure regulation), and neurotransmission (Moncada et al., 1991). The potential for overproduction of NO in the body to have adverse effects on health is due largely to intermediates formed during its reactions with molecular oxygen or superoxide anion (O_2^-) (Tamir and Tannenbaum, 1996); O_2^- is a byproduct of aerobic metabolism in many cell types. Despite intense investigation of the biological effects of NO in recent years, very little quantitative information has emerged on the concentrations of the various intermediates, and especially their spatial distribution relative to a source of NO in vivo or in vitro. Among the factors that have made it difficult to quantitate the rate processes in the vicinity of NO-producing cells are the complex chemistry of nitrogen oxides in aqueous solutions and the extremely low concentrations of key intermediates such as nitrous anhydride (N_2O_3) and peroxynitrite.

There have been few attempts to model the coupling between the reaction and diffusion of NO in cells or tissues. Lancaster (1994, 1996) simulated the diffusion of endogenously produced NO, approximating its consumption in tissues as being due to one or more first-order processes. This was sufficient to reach certain conclusions about the distribution of NO itself, but did not yield information about the reaction products or intermediates of interest here. Similarly, Wood and Garthwaite (1994) used a simple, first-order decay process in their models describing the diffusion of NO generated from single or multiple sources.

Lewis et al. (1995a) measured the rate of release of NO by activated macrophages in vitro, along with the rates of formation of the principal products in the extracellular fluid. Macrophages attached to microcarrier beads were studied in suspension cultures in the stirred vessel shown schematically in Fig. 1 *a*. The concentration of NO in the culture medium was monitored continuously by a chemiluminescence detector, and the concentrations of NO_2^- and NO_3^-, the main end products of NO oxidation, were measured at discrete times. Superoxide dismutase (SOD, which scavenges O_2^-) was added to the culture medium in some experiments, and morpholine (a model amine) was present in others. The concentration of N-nitrosomorpholine was monitored in the latter as an indication of the ability to form nitrosamines (many of which are carcinogenic) from N_2O_3. It was found that NO production by the macrophages started 2–5 h after cell activation and that the NO concentration reached a steady state after ~9 h. At that time, NO_2^- and NO_3^- were formed at approximately equal and constant rates. The theoretical analysis was limited in that it assumed

Received for publication 2 February 1998 and in final form 7 May 1998.
Address reprint requests to William M. Deen, Department of Chemical Engineering, Room 66-572, Massachusetts Institute of Technology, Cambridge, MA 02139. Tel.: (617) 253-4535; Fax: (617) 258-8224; E-mail: wmdeen@mit.edu.

0006-3495/98/08/745/10 $2.00

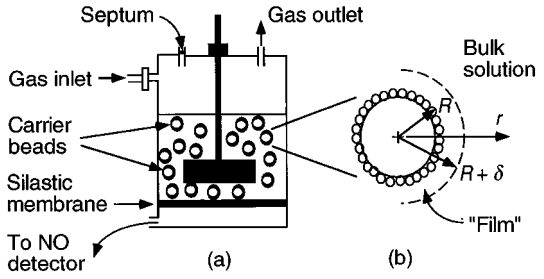

FIGURE 1 Schematic of macrophage culture system used by Lewis et al. (1995a): (*a*) stirred suspension in reactor; (*b*) enlargement showing a single microcarrier bead covered by a monolayer of cells.

that the entire extracellular solution was well mixed. Thus, many of the important chemical events were considered, but the model did not account for the finite rates of diffusion of NO and its reaction products.

The objective of the present study was to develop a mathematical model to simulate the interaction between diffusion and the complex chemistry of NO in biological solutions. To permit comparisons with experimental data, the analysis focused specifically on the macrophage suspension cultures used by Lewis et al. (1995a). The results reveal some of the important concentration and length scales, and offer insight into the critical roles of CO_2 and bicarbonate in the solution chemistry of NO.

MODEL FORMULATION

Overview

The analysis focused on the fluid surrounding a representative microcarrier bead. As shown in Fig. 1 *b*, the culture medium was assumed to consist of two regions. Most of the extracellular volume was regarded as a well-mixed solution, whereas the resistance to mass transfer between the macrophages and the culture medium was described using a stagnant-film model. Thus, there was a region adjacent to a given carrier bead (the "film") in which species concentrations were dependent on position. Different events were found to predominate in the film and bulk regions, as will be discussed. The main extracellular processes that were represented are depicted in Fig. 2; reactions are indicated by solid arrows and diffusion by dashed arrows. Both NO and O_2^- are synthesized within the cells and enter the culture medium. It is well established that NO reacts with O_2 to give N_2O_3 and, ultimately, NO_2^-. It is also well known that NO reacts with O_2^- to form peroxynitrite ($ONOO^-$), the acid form of which rearranges to give NO_3^-. The decomposition of peroxynitrite provides an additional source of NO_2^-, as does the reaction of NO with peroxynitrite. Although not shown specifically in Fig. 2, the catalytic effects of CO_2 and certain anions are included in the kinetic model described below.

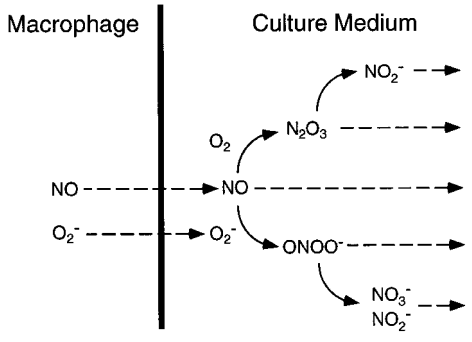

FIGURE 2 The main reaction and diffusion processes included in the model. Reactions and diffusional steps are indicated by solid and dashed lines, respectively.

Presented next is a more detailed discussion of the reactions, followed by the governing equations for the film and bulk regions and a brief description of the numerical methods.

Reaction scheme

The oxidation of NO by molecular oxygen, in which nitrite is the final product, is described by

$$2NO + O_2 \xrightarrow{k_1} 2NO_2 \tag{1}$$

$$NO + NO_2 \underset{k_{-2}}{\overset{k_2}{\rightleftharpoons}} N_2O_3 \tag{2}$$

$$N_2O_3 + H_2O \xrightarrow{k_3} 2NO_2^- + 2H^+ \tag{3}$$

where k_i is the rate constant for reaction *i*. The overall rate of NO oxidation by this pathway is controlled by reaction 1 (Lewis and Deen, 1994). An important observation is that the hydrolysis of nitrous anhydride (reaction 3) also takes place in concert with certain anions, namely bicarbonate (HCO_3^-), chloride, and one or more forms of inorganic phosphate (Lewis et al., 1995b; Caulfield et al., 1996). All of these were present in the culture medium. Representing these anions as X^-, the anion-catalyzed hydrolysis is written as

$$N_2O_3 + X^- \xrightarrow{k_4} NO_2^- + NOX \xrightarrow{H_2O} 2NO_2^- + X^- + 2H^+ \tag{4}$$

where the overall rate is controlled by the formation of the nitrosyl compound (NOX). The main effect of reaction 4 is to reduce the concentration of N_2O_3, the agent responsible for the formation of N-nitroso compounds (see below).

When superoxide is present, an alternative pathway for NO oxidation is (Koppenol et al., 1992; Huie and Padmaja, 1993)

$$NO + O_2^- \xrightarrow{k_5} ONOO^- \tag{5}$$

$$ONOOH \xrightarrow{k_6} NO_3^- + H^+. \tag{6}$$

In this case the end product is nitrate, rather than nitrite. Because it involves the combination of two radicals, reaction 5 is extremely fast. As shown in reaction 6, it is the protonated form of peroxynitrite (i.e., peroxynitrous acid) which decomposes; peroxynitrite is stable at high pH because almost all of it is present then as the anion. It has been reported recently by Pfeiffer et al. (1997) that the decomposition of peroxynitrite also produces nitrite. A detailed mechanism was proposed by those authors, but a simple representation of their findings adequate for our simulations is

$$ONOOH \xrightarrow{k_7} NO_2^- + \frac{1}{2}O_2 + H^+. \tag{7}$$

Competing with NO for superoxide are the catalyzed and uncatalyzed dismutation reactions (Fielden et al., 1974; Imlay and Fridovich, 1991),

$$O_2^- + H_2O \xrightarrow[\text{SOD}]{k_8} \frac{1}{2}O_2 + \frac{1}{2}H_2O_2 + OH^- \quad (8)$$

$$HO_2 + O_2^- + H_2O \xrightarrow{k_9} O_2 + H_2O_2 + OH^-. \quad (9)$$

In the macrophage study of Lewis et al. (1995a), SOD was added to the culture medium only in certain experiments, so that reaction 8 was not always present. Reaction 9 is slow enough that it was always much less important for the consumption of superoxide than reaction 5, but it is included here for completeness.

Another recent finding is that the conversion of peroxynitrite to nitrate is accelerated by the reaction of $ONOO^-$ with CO_2 (Denicola et al., 1996; Lymar and Hurst, 1995; Uppu et al., 1996),

$$ONOO^- + CO_2 + H_2O \xrightarrow{k_{10}} NO_3^- + CO_3^{2-} + 2H^+. \quad (10)$$

As pointed out in the studies just cited, under physiological conditions reaction 10 is faster than reaction 6. An additional mechanism for nitrite formation is the reaction of NO with peroxynitrite (Pfeiffer et al., 1997),

$$NO + ONOO^- \xrightarrow{k_{11}} NO_2^- + NO_2. \quad (11)$$

In this case the available data do not indicate which form of peroxynitrite is reactive, so that writing $ONOO^-$ rather than ONOOH in reaction 11 is arbitrary. Another reaction of interest in the macrophage study was the nitrosation of morpholine. The N-nitrosation of a secondary amine (R_2NH) at physiological pH is represented as

$$N_2O_3 + R_2NH \xrightarrow{k_{12}} R_2NNO + NO_2^- + H^+. \quad (12)$$

Notice that N_2O_3 is the nitrosating agent under these conditions, and that it is the uncharged form of the amine (e.g., morpholine), which is reactive. N-nitrosomorpholine, represented in reaction 12 as R_2NNO, will be denoted also as NMor.

The list of reactions is completed by the acid-base equilibria,

$$ONOOH \overset{K_{13}}{\rightleftharpoons} ONOO^- + H^+ \quad (13)$$

$$CO_2 + H_2O \overset{K_{14}}{\rightleftharpoons} HCO_3^- + H^+ \quad (14)$$

$$HO_2 \overset{K_{15}}{\rightleftharpoons} O_2^- + H^+ \quad (15)$$

$$R_2NH_2^+ \overset{K_{16}}{\rightleftharpoons} R_2NH + H^+ \quad (16)$$

where K_i is the equilibrium (acid dissociation) constant. An assumption implicit in reaction 14 is that carbonic acid (H_2CO_3) and CO_2 are in equilibrium. Not included are the equilibria involving carbonate or nitrous acid, because the respective pK values are too extreme for them to be significant (9.9 for CO_3^{2-}/HCO_3^- and 3.4 for NO_2^-/HNO_2). The phosphate equilibria (e.g., $HPO_4^{2-}/H_2PO_4^-$) also were not used, because the available rate expression for reaction 4 with phosphate is based on the *total* phosphate concentration at pH 7.4 (Lewis et al., 1995b), and it is not yet clear which form(s) of phosphate are involved.

Film region

The simulations focused on the period beginning several hours after macrophage activation, when the NO concentration was constant. Thus, the reactants and intermediates were essentially at steady state, while the amounts of the final products increased continuously with time. In spherical coordinates, the stagnant film adjacent to a carrier bead was assumed to extend from a radial position $r = R$ (corresponding to the outer edge of a monolayer of macrophages) to $r = R + \delta$. The concentrations were assumed to be independent of the spherical angles, so that the species conservation equation was

$$\frac{D_i}{r^2}\frac{\partial}{\partial r}\left(r^2\frac{\partial C_i}{\partial r}\right) + R_i = 0 \quad (17)$$

where C_i is the molar concentration of species i, D_i is its diffusivity, and R_i is its local rate of formation by reaction, per unit volume (Deen, 1998). The net rate of formation of any species is calculated by summing the rates of all reactions in which it participates, yielding position-dependent values of R_i which may be either positive or negative.

Equation 17 was used only for three key species: NO, O_2^-, and total peroxynitrite (Per, the sum of $ONOO^-$ and ONOOH). The position-dependent concentrations of NO_2 and N_2O_3 were calculated from algebraic equations given below, whereas the concentrations of most other species were assumed to be spatially uniform. Specified as inputs were the concentrations of H^+, O_2, CO_2, Cl^-, phosphate, SOD, and morpholine. The HCO_3^- concentration was calculated from the CO_2 concentration and pH. It is worth noting that CO_2 and HCO_3^- both act as catalysts; that is, reaction 4 (with $X^- = HCO_3^-$) and reaction 10 do not cause net consumption of "total CO_2." The measured conversion of morpholine to NMor was <0.2% (Lewis et al., 1995a), so that the total morpholine concentration did not change significantly over the course of an experiment. However, it was observed that the pH decreased gradually, so that the concentrations of all species involved in acid-base equilibria were time-dependent. The acidification was slow enough that the system was pseudosteady; that is, there was no need to include a time derivative in Eq. 17.

Based on the reactions given above, the rates of formation of NO_2 and N_2O_3 are

$$R_{NO_2} = 2k_1C_{NO}^2C_{O_2} - k_2C_{NO}C_{NO_2} + k_{-2}C_{N_2O_3} + k_{11}C_{NO}C_{Per} \quad (18)$$

$$R_{N_2O_3} = k_2C_{NO}C_{NO_2} - k_{-2}C_{N_2O_3} - k_3C_{N_2O_3} - \sum k_4^X C_{X^-}C_{N_2O_3} - k_{12}C_{N_2O_3}C_{Mor^0}. \quad (19)$$

The summation involving k_4 in Eq. 19 (and subsequent relations) is over all participating anions and Mor^0 denotes the *uncharged* form of morpholine (i.e., R_2NH in reaction 12). The neutral form of morpholine is related to total morpholine (Mor, the sum of R_2NH and $R_2NH_2^+$) by

$$C_{Mor^0} = \frac{C_{Mor}}{1 + 10^{pK_{16}-pH}}. \quad (20)$$

The concentrations of NO_2 and N_2O_3, both trace intermediates, were evaluated by setting $R_i = 0$ in Eqs. 18 and 19. (This is akin to the quasi-steady-state approximation often invoked for closed, batch reactors.) The resulting expressions were

$$C_{NO_2} = \left(1 + \frac{k_{-2}}{k_3 + \sum k_4^X C_{X^-} + k_{12}C_{Mor^0}}\right) \cdot \left(\frac{2k_1C_{NO}C_{O_2} + k_{11}C_{Per}}{k_2}\right) \quad (21)$$

$$C_{N_2O_3} = \frac{2k_1C_{NO}^2C_{O_2} + k_{11}C_{NO}C_{Per}}{k_3 + \sum k_4^X C_{X^-} + k_{12}C_{Mor^0}}. \quad (22)$$

Using this information, the rates of formation of the key species were found to be

$$R_{NO} = -4k_1C_{NO}^2C_{O_2} - k_5C_{NO}C_{O_2^-} - 2k_{11}C_{NO}C_{Per} \quad (23)$$

$$R_{O_2^-} = -k_5C_{NO}C_{O_2^-} - k_8C_{O_2^-}C_{SOD} - k_9C_{HO_2}C_{O_2^-} \quad (24)$$

$$R_{Per} = k_5C_{NO}C_{O_2^-} - (k_6 + k_7)C_{ONOOH} - k_{10}C_{CO_2}C_{ONOO^-} - k_{11}C_{NO}C_{Per}. \quad (25)$$

The concentrations of peroxynitrite anion, peroxynitrous acid, and total peroxynitrite are related by

$$C_{ONOO^-} = \frac{C_{Per}}{1 + 10^{pK_{13}-pH}} \equiv fC_{Per}, \quad C_{ONOOH} = (1-f)C_{Per}. \quad (26)$$

At a representative pH of 7.2, the fraction present as the anion (f) is 0.74.

Two boundary conditions were needed for Eq. 17 for each of the key species. The fluxes of NO and O_2^- at the cell surface were specified based on the experimental data, whereas the flux of peroxynitrite was assumed to be zero. Thus,

$$\left.\frac{\partial C_i}{\partial r}\right|_{r=R} = -\frac{N_i|_{r=R}}{D_i}, \quad i = \text{NO or } O_2^- \quad (27)$$

$$\left.\frac{\partial C_{Per}}{\partial r}\right|_{r=R} = 0 \quad (28)$$

where N_i is the radial component of the molar flux of species i. At $r = R + \delta$ it was required that the concentrations in the film match those in the bulk solution ($C_{i,b}$), or

$$C_i|_{r=R+\delta} = C_{i,b}. \quad (29)$$

This completes the formulation for the film region.

Bulk solution

In the bulk solution there is a balance among mass transfer from the film regions, formation by reaction, and physical losses from the system. Thus, the pseudosteady conservation equation for the key species is

$$4\pi n(R+\delta)^2 N_i|_{r=R+\delta} + R_{i,b} - h_iC_{i,b} = 0 \quad (30)$$

where n is the number of microcarrier beads per unit volume of bulk solution, $R_{i,b}$ is the rate of formation of species i in this region, and h_i describes the losses of species i to the gas phase and to the chemiluminescence detector. The reaction rates were calculated using expressions analogous to those given above for the film. Physical losses to the head space and detector were significant only for NO (Lewis et al., 1995a). The film and bulk problems were coupled by Eq. 29 and by the fact that the flux in Eq. 30 had to be evaluated from the concentrations profile in the film (as in Eq. 27).

Rates of product formation

The local rates of formation of the final products are

$$R_{NO_2^-} = 2Ak_1C_{NO}^2C_{O_2} + k_7C_{ONOOH} + (A+1)k_{11}C_{NO}C_{Per} \quad (31)$$

$$R_{NO_3^-} = k_6C_{ONOOH} + k_{10}C_{CO_2}C_{ONOO^-} \quad (32)$$

$$R_{NMor} = k_{12}C_{N_2O_3}C_{Mor^0} \quad (33)$$

$$A = \frac{2k_3 + 2\sum k_4^X C_{X^-} + k_{12}C_{Mor^0}}{k_3 + \sum k_4^X C_{X^-} + k_{12}C_{Mor^0}}. \quad (34)$$

If the amount of N_2O_3 consumed in nitrosating morpholine is negligible relative to N_2O_3 hydrolysis, then $A = 2$. This is very nearly true for the conditions of interest, where it is estimated that $A = 1.9$. Using Eqs. 31–34 to evaluate the reaction rates in the film and bulk regions, the observable rate of increase in the concentration of product species i is

$$\frac{d\langle C_i\rangle}{dt} = \frac{V_b}{V}\left(4\pi n\int_R^{R+\delta} R_i r^2 dr + R_{i,b}\right) \quad (35)$$

where $\langle C_i\rangle$ is the average concentration in the extracellular solution, V_b is the volume in the bulk fluid region, and V is total solution volume.

Numerical methods

The second-order differential equations for the film region were decomposed into pairs of first-order equations, which were solved using a finite-difference relaxation method given by Press et al. (1972). For most of the results to be reported, the film was divided into 100 intervals. The system of nonlinear algebraic equations describing the bulk solution was solved using a globally convergent Newton's iteration scheme (Press et al., 1972).

The first step in solving the combined problem was to assume values for the bulk concentrations of the various species. The film equations were solved using these initial guesses, and the fluxes at the outer edge of the film calculated for use in Eq. 30. The bulk solution model was then solved again, and the iterative process repeated until the calculated values of the bulk concentrations did not change significantly (a fractional difference between two successive steps of $<10^{-5}$). To compute the rates of product formation, the integral in Eq. 35 was evaluated using Simpson's rule. The effects of the gradual acidification were simulated by computing all quantities at several values of pH, and using Simpson's rule to integrate over time.

RESULTS

Parameter values

The measured or estimated values of the physicochemical constants at pH 7.4 and 37°C are summarized in Table 1. The value of k_4 for nucleophile X is denoted as k_4^X. The results of Koppenol et al. (1992) were used for the total rate of peroxynitrite decomposition ($k_6 + k_7 = 4.5\ s^{-1}$), whereas the ratio k_6/k_7 was estimated from the data of Pfeiffer et al. (1997). In a few instances the rate constants were available only at room temperature or at a different pH. This was true for k_2 and k_{-2} (20°C), k_3 (25°C), and k_4 for HCO_3^- (25°C and pH 8.9). In the absence of other data, the aqueous diffusivities for superoxide and peroxynitrite were assumed to equal those for oxygen (Goldstick and Fatt, 1970) and nitrate (Newman, 1973), respectively. Those values were adjusted to 37°C by assuming that $D_i\mu/T$ is constant, where μ is the viscosity of water and T is absolute temperature. In several entries in Table 1 the number of digits probably exceeds what is justified experimentally, but the digits

TABLE 1 Physicochemical constants (at 37°C and pH 7.4)

Quantity	Value	Reference
k_1	2.4×10^6 M^{-2} s^{-1}	Lewis and Deen (1994)
k_2	1.1×10^9 M^{-1} s^{-1}	Schwartz (1983)
k_{-2}	4.3×10^6 s^{-1}	Licht et al. (1988), Schwartz (1983)
k_3	1.6×10^3 s^{-1}	Licht et al. (1988)
k_4^{Pi}	8.3×10^5 M^{-1} s^{-1}	Lewis et al. (1995b)
k_4^{Cl}	1.6×10^5 M^{-1} s^{-1}	Lewis et al. (1995b)
$k_4^{HCO_3}$	1.5×10^6 M^{-1} s^{-1}	Caulfield et al. (1996)
k_5	6.7×10^9 M^{-1} s^{-1}	Huie and Padmaja (1993)
k_6	3.1 s^{-1}	See text
k_7	1.4 s^{-1}	See text
k_8	2.5×10^9 M^{-1} s^{-1}	Fielden et al. (1974)
k_9	8×10^7 M^{-1} s^{-1}	Imlay and Fridovich (1991)
k_{10}	2.9×10^4 M^{-1} s^{-1}	Lymar and Hurst (1995)
k_{11}	9.1×10^4 M^{-1} s^{-1}	Pfeiffer et al. (1997)
k_{12}	5.0×10^7 M^{-1} s^{-1}	Lewis et al. (1995b)
pK_{13}	6.75	Koppenol et al. (1992)
pK_{14}	6.10	Davenport (1974)
pK_{15}	4.8	Fridovich (1978)
pK_{16}^{Mor}	8.23	Hetzer et al. (1966)
D_{NO}	5.1×10^{-5} cm^2/s	Wise and Houghton (1968)
$D_{O_2^-}$	2.8×10^{-5} cm^2/s	See text
D_{Per}	2.6×10^{-5} cm^2/s	See text

shown were retained to minimize roundoff errors. There is a considerable range of reported values for k_3, for example, as discussed in Licht et al. (1988).

The values of the parameters that were specific to the macrophage experiments of Lewis et al. (1995a) are shown in Table 2. The radius of $R = 95$ μm is based on the average hydrated diameter of the microcarrier beads (175 μm) and an allowance for the thickness of a cell monolayer. The effective film thickness was calculated from an estimate of the mass transfer coefficient (k_c) for NO. Using the correlation of Asai et al. (1988) for particles in an agitated vessel, the Sherwood number (Sh) for NO is given by

$$Sh = \frac{k_c d}{D_{NO}} = [2^{5.8} + \{0.61(\epsilon^{1/3} d^{4/3}/\nu)^{0.58} Sc^{1/3}\}^{5.8}]^{1/5.8} \qquad (36)$$

TABLE 2 Parameters for macrophage cultures (Lewis et al., 1995a)

Quantity	Value
R	95 μm
δ	63 μm
n	1.43×10^3 beads/ml
V_b	98.2 ml
V_f	1.85 ml
h_{NO}	7.5×10^{-4} s^{-1}
C_{O_2}	200 μm
C_{CO_2}	1.14 mM
C_{Pi}	0.9 mM
C_{Cl}	110 mM
C_{HCO_3}	23–9 mM
C_{Mor} (when present)	1.0 mM
C_{SOD} (when present)	3.2 μM
pH	7.4–7.0
$N_{NO}\|_{r=R}$	3.1×10^{-8} mol s^{-1} m^{-2}
$N_{O_2^-}\|_{r=R}$	1.5×10^{-8} mol s^{-1} m^{-2}

where ϵ is proportional to the rate of input of mechanical energy, ν is the kinematic viscosity, $d(= 2R)$ is the particle diameter, and Sc $(= \nu/D_{NO})$ is the Schmidt number for NO. Using $\epsilon = 30$ cm^2 s^{-3} (based on a correlation in Nagata, 1975) and $Sc = 136$, we obtained $Sh = 5.04$. The effective film thickness for spherical coordinates is then $\delta = 2R/(Sh - 2) = 63$ μm. The concentration of beads (n) was based on 400 mg of hydrated beads per 100 ml, with the bead density assumed to be that of water. In calculating the bulk (V_b) and film (V_f) contributions to the extracellular fluid volume, it was assumed that $V (= V_b + V_f)$ equaled the total liquid volume of 100 ml; that is, the bead and cell volumes were neglected. The CO_2 concentration was calculated from the partial pressure of $0.05 \times (760) = 38$ mmHg and the CO_2 solubility in blood plasma, 3.01×10^{-5} M $mmHg^{-1}$ (Davenport, 1974). The HCO_3^- concentration was then calculated using pK_{14} and the specified pH. In the macrophage culture experiments there was a linear decline in pH over time, from 7.4 to ~7.0. Simulations were performed both for constant pH and with this linear decline. The flux of NO from the cells to the surrounding fluid was based on the average total release rate of 6.0 pmol s^{-1} $(10^6$ cells$)^{-1}$, the average viable cell count of 0.83×10^6 cells/ml, and the aforementioned estimates of the number and size of the beads. The flux of O_2^- from the cells was assumed to be one-half that of NO, as deduced by Lewis et al. (1995a) and as measured using similar macrophage cultures (deRojas-Walker et al., 1995).

Concentration and length scales

Before examining the results of the simulations, we can reach some conclusions about the concentration and length scales based on order-of-magnitude considerations. The concentration scales for species i in the film and bulk regions are denoted as C_i^* and $C_{i,b}^*$, respectively. Based on direct measurements of the steady-state NO concentration, $C_{NO,b}^* \cong 1$ μM (Lewis et al., 1995a). An upper bound for the concentration change across the film is $\Delta C_{NO} \cong (N_{NO}|_{r=R})\delta/D_{NO} = 0.4$ μM, indicating that the concentrations for NO in the film and bulk solution were roughly the same. This was not true for superoxide. In fact, almost all of the O_2^- released by the cells must have been consumed within the film, which may be inferred as follows. Suppose that the reaction of O_2^- with NO was such that most O_2^- was consumed within a layer of thickness L_1. It follows that

$$N_{O_2^-}|_{r=R} \sim k_5 L_1 C_{NO}^* C_{O_2^-}^* \qquad (37)$$

where "~" denotes an order-of-magnitude equality. An independent estimate of the flux is

$$N_{O_2^-}|_{r=R} \sim \frac{D_{O_2^-} C_{O_2^-}^*}{L_1}. \qquad (38)$$

Equating these two expressions for the O_2^- flux and solving for L_1 gives

$$L_1 \sim \left(\frac{D_{O_2^-}}{k_5 C^*_{NO}}\right)^{1/2}. \quad (39)$$

Using $C^*_{NO} = 1\ \mu M$ and the data in Table 1 we obtain $L_1 \cong 0.6\ \mu m$, or ~1% of the film thickness. This suggests that almost no superoxide reached the bulk solution. Using this result in Eq. 38, the concentration scale for superoxide in the film is found to be $C^{*-}_{O_2} \cong 3$ nM. This approach does not yield any information about the superoxide concentration in the bulk solution, beyond the conclusion that it was much smaller than in the film.

The magnitude of the peroxynitrite concentration in the film was estimated by assuming that its formation near the cells (where O_2^- was relatively abundant) was balanced by its diffusion and its consumption elsewhere (where O_2^- was virtually absent). Under the conditions of interest, reaction 10 is by far the fastest of those consuming peroxynitrite. Assuming that diffusion and reaction 10 were the dominant rate processes for peroxynitrite over a region of thickness L_2, reasoning like that used to obtain Eq. 39 leads to

$$L_2 \sim \left(\frac{D_{Per}}{k_{10} C_{CO_2} f}\right)^{1/2}. \quad (40)$$

Using the data in Tables 1 and 2 we obtain $L_2 \cong 10\ \mu m$. This suggests that the peroxynitrite-containing region was much thicker than that for superoxide, but that it was still only a small fraction of the film. Thus, as with superoxide, it appears that little peroxynitrite reached the bulk solution. An overall balance between the formation and consumption of peroxynitrite in the film suggests that

$$C^*_{Per} \sim \frac{k_5 C^*_{NO} C^*_{O_2^-} L_1}{k_{10} C_{CO_2} f L_2}. \quad (41)$$

which gives $C^*_{Per} \cong 40$ nM. We conclude that for two key species (O_2^- and Per) there were very different concentration scales in the film and bulk regions. This suggests that large errors in at least some predictions would result if we were to assume the reactor to be perfectly mixed.

Concentration profiles

The actual concentration profiles computed for the key species in the film region (for pH 7.2 and no SOD present) are shown in Fig. 3. In this plot all concentrations are normalized by the values at the cell surfaces. For NO, there was only a 16% drop in concentration across the film, confirming that the film and bulk values were roughly equal. In contrast, the rapid consumption of superoxide (from reaction 5) caused the O_2^- concentration to fall almost to zero over a distance corresponding to only ~3% of the film thickness, or 2 μm. The peroxynitrite concentration declined somewhat more gradually, essentially reaching zero at a distance of ~30 μm. The concentrations of O_2^- and

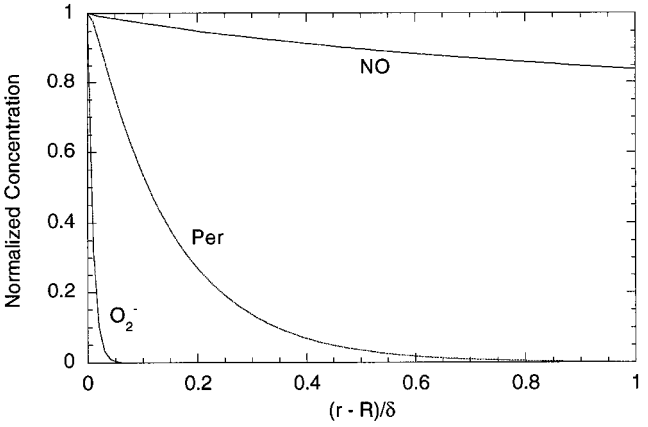

FIGURE 3 Concentration profiles for NO, O_2^-, and total peroxynitrite (Per) in the film region, calculated assuming pH 7.2 and no morpholine or SOD present. In each case the concentration has been normalized by the value adjacent to the cells, which was 1.13 μM for NO, 3.32 nM for O_2^-, and 51 nM for Per.

Per computed at the cell surface (3.3 nM and 51 nM, respectively) are in reasonable agreement with the order of magnitude estimates, as are the length scales for the concentration changes. Moreover, the corresponding concentrations in the bulk solution (0 and 0.53 pM) were extremely small, as expected.

Rates of product formation

Table 3 shows comparisons of several of the model predictions with the data of Lewis et al. (1995a). Included are the concentration of NO, the rates of formation of NO_2^- and NO_3^-, and the rate of loss of NO to the head space. In the experiments where morpholine was added to the culture medium, the amount of NMor formed was too small to have much effect on the overall nitrogen balance, so those results have been combined with the ones for the control conditions (neither Mor nor SOD present). It was found that the time-averaged results of the simulations, based on linear declines in pH, were very similar to the results computed for pH 7.2. Accordingly, the results shown are based on pH 7.2, with the other parameter values as given in Tables 1 and 2. It is seen in Table 3 that the model predictions are in fairly good agreement with the experimental results, especially in view of the fact that no parameters were adjusted to fit the data. In particular, the predicted effect of adding SOD is very similar to what was observed. By scavenging superoxide in the extracellular fluid, SOD reduced the rate of peroxynitrite formation and thereby lowered the NO_3^-/NO_2^- ratio. The ability of the model to accurately predict this effect supports the view that most nitrite and nitrate production was extracellular, as assumed by Lewis et al. (1995a). Although the model predictions were generally satisfactory, note that there was a tendency to underestimate the rate of nitrite formation and overestimate the rate of nitrate formation. Thus, the predicted NO_3^-/NO_2^- ratio tended to be too large,

TABLE 3 Comparisons of the model predictions with the data of Lewis et al. (1995a)

Conditions	$C_{NO,b}$ (μM)	NO_2^- Formation [pmol s^{-1} $(10^6$ cells$)^{-1}$]	NO_3^- Formation [pmol s^{-1} $(10^6$ cells$)^{-1}$]	NO Loss [pmol s^{-1} $(10^6$ cells$)^{-1}$]
Control or with Mor				
Model	0.95	2.2*	3.0	0.86
Data	0.73 ± 0.08	2.7 ± 0.2	2.4 ± 0.3	0.62 ± 0.10
With SOD				
Model	1.2	3.3	1.6	1.1
Data	0.84 ± 0.11	3.8 ± 0.5	1.4 ± 0.2	1.1 ± 0.2

The experimental values are mean ± SE for seven control or morpholine experiments and three with SOD.
*This is the result calculated for the control conditions (no morpholine or SOD); when morpholine was included, the value was 2.1.

especially with SOD absent (1.34 vs. 0.88 ± 0.08 SE without SOD and 0.48 vs. 0.39 ± 0.09 with SOD). The model also overestimated the NO concentration by 0.2–0.3 μM.

The predicted rate of NMor formation was 0.100 pmol s^{-1} $(10^6$ cells$)^{-1}$, or about three times the observed rate of 0.038 ± 0.011. Possible reasons for this discrepancy and for the tendency to overestimate the NO_3^-/NO_2^- ratio are discussed later.

As mentioned in connection with Fig. 3, the model indicates that almost all of the peroxynitrite was formed and consumed within the film regions. Because peroxynitrite is the immediate precursor of nitrate, almost all of the nitrate must have been formed there. Indeed, although the film regions comprised only 2% of the extracellular volume, they were calculated to account for 99.3% of the nitrate synthesis under control conditions. In contrast, 94% of the nitrite formation and 97% of the NMor formation were computed to occur in the bulk solution.

Effects of the O_2^-/NO flux ratio

The ratio of O_2^- to NO release by the cells, which was 0.5 for the conditions studied by Lewis et al. (1995a), is not a fixed constant for a given cell line. Rather, it is expected to depend on such environmental factors as the method used to induce NO synthase and the levels of L-arginine and dissolved oxygen. Fig. 4 shows the predicted effect of this flux ratio on the relative amounts of nitrate and nitrite formed. Curves are shown for the NO flux given in Table 2, and for a flux one-third of that value, corresponding to a hypothetical situation with less induction of NO synthase. It is seen that the NO_3^-/NO_2^- concentration ratio increases exponentially as the O_2^-/NO flux ratio is increased. This is because peroxynitrite formation is favored when superoxide is relatively abundant, and most peroxynitrite decomposes to NO_3^-. The NO_3^-/NO_2^- ratio is somewhat larger at the lower NO flux, because NO_3^- production is first-order in NO, whereas NO_2^- formation is approximately second-order. Thus, the lower NO flux, which lowers the NO concentration, favors formation of NO_3^-. Variations in the relative rates of O_2^- and NO release may largely explain the differing NO_3^-/NO_2^- ratios reported for macrophage cultures (Iyengar et al., 1987; Lewis et al., 1995a).

DISCUSSION

This study represents an initial attempt to describe the interaction between diffusion and the complex chemistry of NO in biological solutions. As noted already, previous simulations of NO diffusion in tissues (Lancaster, 1994, 1996; Wood and Garthwaite, 1994) focused on describing the concentration of NO itself, and did not attempt to predict the rates of formation or the spatial distribution of the

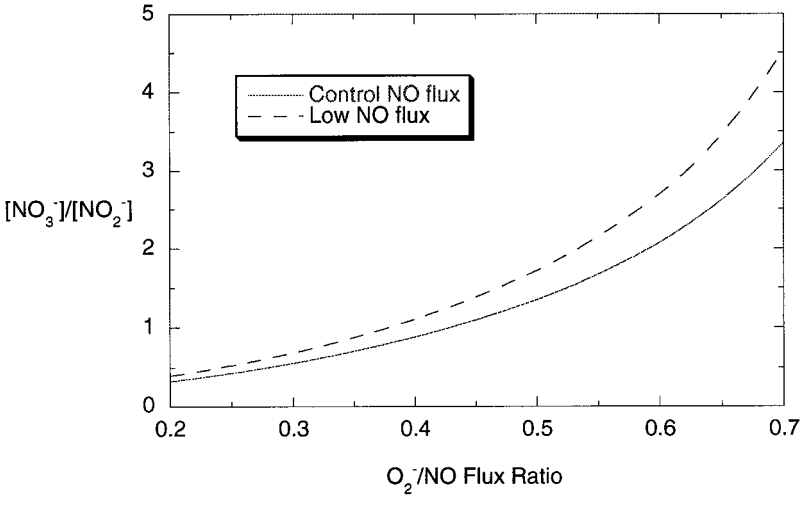

FIGURE 4 Effect of the relative cellular release rates of O_2^- and NO on the relative amounts of NO_3^- and NO_2^- formed. The abscissa is a ratio of fluxes and the ordinate a ratio of concentrations. Results are shown for the NO flux in Table 2 ("Control NO flux") and for a flux which was one-third of that value ("Low NO flux").

various species resulting from NO oxidation. Two of the intermediates in the NO oxidation pathways, N_2O_3 and peroxynitrite, are of special interest because of their cytotoxic and mutagenic properties (Tamir and Tannenbaum, 1996). Although it has not been possible to directly measure the concentrations of these trace intermediates in cell cultures, one should be able to make useful inferences by examining the principal end products, namely, NO_2^-, NO_3^-, and (where present) NMor. Our objective was to develop a mathematical model that would permit such inferences. To test the model, we focused on the experimental results of Lewis et al. (1995a) obtained using suspension cultures of activated macrophages.

Using the chemical pathways and rate constants known at the time, and modeling the extracellular fluid as a well-mixed compartment, Lewis et al. (1995a) noted two major discrepancies between their measurements and predictions. The first was that the rate of NO_2^- formation predicted from the reaction of NO with O_2 (reactions 1–4) accounted for only about half the amount of NO_2^- observed experimentally. The second was that the predicted rate of N-nitrosomorpholine (NMor) formation was about six times too large. The reactor model used here is an improvement over that used by Lewis et al. (1995a), in that it distinguishes between film and bulk regions. The reaction scheme is also more complete. The "new" reactions included here are 1) the formation of NO_2^- from NO and peroxynitrite (reaction 11); 2) the formation of NO_2^- from peroxynitrite decomposition (reaction 7); 3) the catalysis of peroxynitrite decomposition by CO_2 (reaction 10); and 4) the facilitation of N_2O_3 hydrolysis by bicarbonate (reaction 4 with $X^- = HCO_3^-$). Of these, reaction 11 was proposed by Lewis et al. (1995a) as an explanation for the excess NO_2^- formation they measured, but no independent rate information was available to test that hypothesis. The other reactions just listed were not yet known.

The contributions of the first three new reactions can be assessed by examining their individual effects on the predicted ratio of nitrate to nitrite formation for the control conditions (i.e., without SOD). These effects are shown in Fig. 5. When none of the new reactions was included (case A), the predicted nitrate/nitrite ratio was 1.40, significantly greater than the experimental value of 0.88 ± 0.08. Adding reaction 11 alone (case B) lowered the nitrate/nitrite ratio to 1.17, and including both reactions 11 and 7 (case C) decreased it further to 0.60. Thus, the combined effect of the reactions studied by Pfeiffer et al. (1997), which yield nitrite either from the combination of NO and peroxynitrite or from peroxynitrite decomposition, was to lower the calculated nitrate/nitrite ratio from a level well above to a level well below the experimental value. However, including reaction 10 (case D, the complete model) increased the nitrate/nitrite ratio back to 1.34. This suggests that the CO_2-catalyzed decomposition of peroxynitrite (to give NO_3^-) is fast enough to make the other peroxynitrite reactions unimportant. This is confirmed by simulations in which only reaction 10 was added to the basic scheme (case E); the resulting nitrate/nitrite ratio of 1.40 was identical to that with the basic scheme and only slightly above that for the full model (1.34). We conclude that the reactions reported subsequent to the work of Lewis et al. (1995a) do not provide an explanation for the relatively high rate of nitrite formation (or low nitrate/nitrite ratio) that was observed.

A factor that has not been considered in attempting to rationalize the observed nitrate/nitrite ratio is the possibility that extracellular peroxynitrite may have entered the cells and/or reacted with some component of the cell membrane (e.g., the lipids). That is, in the model the peroxynitrite flux at the cell surface was assumed to be zero (Eq. 28). If in reality there was a flux of peroxynitrite toward the cells, due either to membrane permeation or reaction, it would have diverted some of the peroxynitrite from the extracellular fluid. This would have preferentially lowered the rate of nitrate formation and thereby lowered the nitrate/nitrite ratio. There are not yet adequate data with which to test this hypothesis.

The other new reaction (reaction 4 with HCO_3^-) mainly influences the rate of NMor formation. In general, the effect

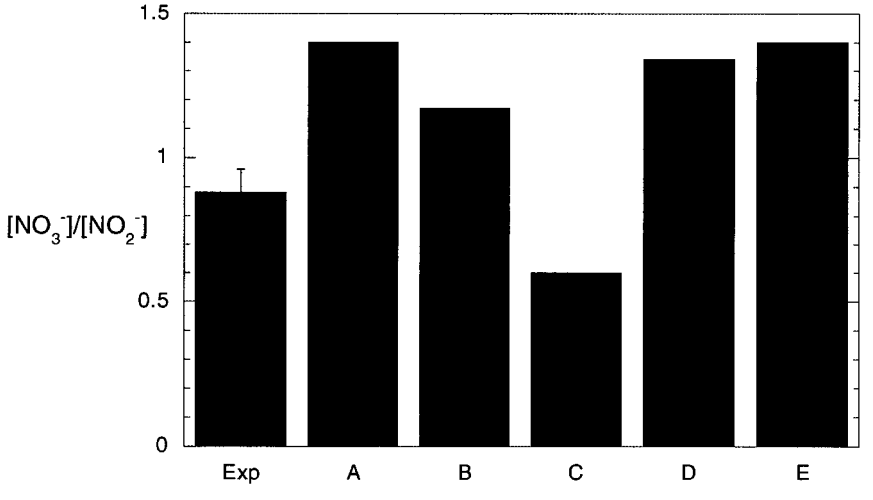

FIGURE 5 Effects of individual reactions on the relative amounts of NO_3^- and NO_2^- formed. The experimental results of Lewis et al. (1995a) (mean ± SE) are denoted by "Exp"; "A" is a basic reaction scheme which excludes reactions 7, 10, and 11 and assumes that $k_6 = 4.5\ s^{-1}$; "B" is the basic scheme plus reaction 11, with $k_6 = 4.5\ s^{-1}$; "C" is the basic scheme plus reactions 7 and 11; "D" is the complete model; and "E" is the basic scheme plus reaction 10. Unless otherwise indicated, the parameter values used were those given in Tables 1 and 2.

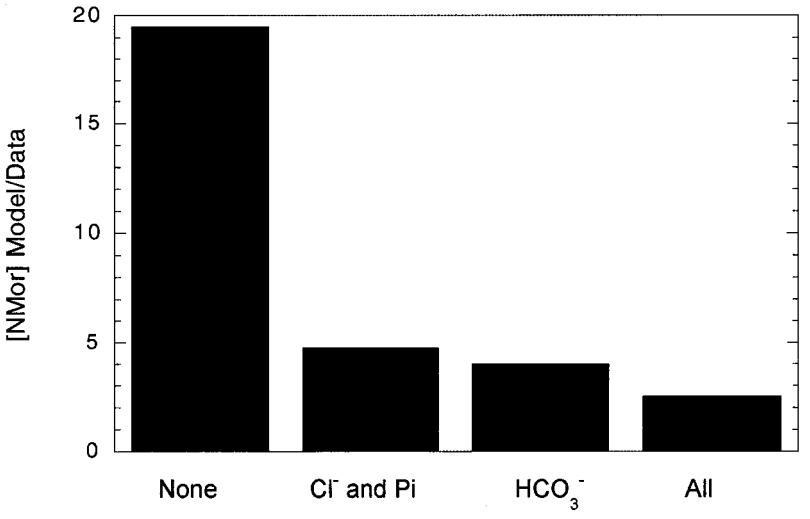

FIGURE 6 Effects of various anions on the predicted rate of N-nitrosomorpholine (NMor) formation, relative to that measured by Lewis et al. (1995a). The labels indicate which anions were included via reaction 4. Inorganic phosphate is denoted as Pi.

of the anion-catalyzed hydrolysis is to reduce the concentration of N_2O_3. Because N_2O_3 is the agent responsible for N-nitrosation under these conditions, this is detectable as a reduction in the rate of NMor formation. The influence of the anions on NMor formation is depicted in Fig. 6. When the anion effects were ignored, the predicted rate of NMor formation was ~20 times too large. When chloride and phosphate were included this factor dropped to 5, similar to the discrepancy noted by Lewis et al. (1995a). Almost all of this calculated change was due to chloride, the phosphate concentration in the cell culture medium being too small to have much effect. The inclusion of bicarbonate reduced the overprediction to a factor of 3. Including bicarbonate, but not chloride or phosphate, the overprediction factor was 4. Thus, the effects of chloride and bicarbonate are quite significant, and roughly comparable to one another. Because almost all of the NMor is predicted to be formed in the bulk solution, very similar results are obtained by treating the reactor as a well-mixed solution, as done previously (Lewis et al., 1995a; Caulfield et al., 1996). The remaining discrepancy between the predicted and observed rates of NMor formation is presumably due to the reaction of N_2O_3 with some other constituent(s) present in the cell culture.

The set of reactions used here to describe the various nitrogen oxide species, while sizable, is probably incomplete. For example, it has been suggested that O_2^- may react with ONOOH to yield NO_2 and O_2 (Miles et al., 1996). Although the magnitude of the rate constant is unknown, this reaction might be significant in situations where cellular production of O_2^- exceeds that of NO.

In conclusion, a mathematical model was developed to describe how rates of reaction and diffusion jointly determine the amounts of the various extracellular products formed from NO in a macrophage culture system. The coupling between reaction and diffusion was found to be especially influential for superoxide and peroxynitrite, which were predicted to be present in significant amounts only in thin layers of solution adjacent to the cells. An interesting implication of this prediction is that, for this particular system, any toxic effects of peroxynitrite would have been experienced only by the cells producing it (or those immediately adjacent). In other words, there appears to have been little or no exchange of peroxynitrite among cells on different carrier beads. In contrast to the very localized production and consumption of peroxynitrite, N_2O_3 appears to have been formed everywhere and distributed more or less uniformly. The N_2O_3 concentrations were very similar in the film and bulk regions because of the relative uniformity of the NO and O_2 concentrations (see Eq. 22). Thus, all cells in the system were potentially exposed to the N_2O_3 generated by any one cell. Such considerations of the spatial distribution of biologically active intermediates may be crucial, for example, when interpreting toxicity or mutagenicity data obtained from mixed cultures of NO "generator" and "target" cells.

The authors are grateful to Dr. Randy S. Lewis for a number of helpful suggestions, including the method used to evaluate the effective film thickness. This work was supported by National Cancer Institute Grant PO1-CA26731.

REFERENCES

Asai, S., Y. Konishi, and Y. Sasaki. 1988. Mass transfer between fine particles and liquids in agitated vessels. *J. Chem. Eng. Jpn.* 21:107–112.

Caulfield, J., S. P. Singh, J. S. Wishnok, W. M. Deen, and S. R. Tannenbaum. 1996. Bicarbonate inhibits N-nitrosation in oxygenated nitric oxide solutions. *J. Biol. Chem.* 271:25859–25863.

Davenport, H. W. 1974. The ABC of Acid-Base Chemistry. 6th ed. University of Chicago Press, Chicago. 41.

Deen, W. M. 1998. Analysis of Transport Phenomena. Oxford University Press, New York. 45.

Denicola, A., B. A. Freeman, M. Trujillo, and R. Radi. 1996. Peroxynitrite reaction with carbon dioxide/bicarbonate: kinetics and influence on peroxynitrite mediated oxidations. *Arch. Biochem. Biophys.* 333:49–58.

deRojas-Walker, T., S. Tamir, H. Ji, J. S. Wishnok, and S. R. Tannenbaum. 1995. Nitric oxide induces oxidative damage in addition to deamination in macrophage DNA. *Chem. Res. Toxicol.* 8:473–477.

Fielden, M. E., P. B. Roberts, R. C. Bray, D. J. Love, G. N. Maunter, G. Rotilio, and L. Calabrese. 1974. The mechanism of action of superoxide

dismutase from pulse radiolysis and electron paramagnetic resonance. *Biochem. J.* 139:49–60.

Fridovich, I. 1978. The biology of oxygen radicals. *Science.* 201:875–880.

Goldstick, T. K., and I. Fatt. 1970. Diffusion of oxygen in solutions of blood proteins. *Chem. Eng. Prog. Symposium Ser. 99.* 66:101–107.

Hetzer, H. B., R. G. Bates, and R. A. Robinson. 1966. Dissociation constant of morpholinium ion and related thermodynamic quantities from 0 to 50°. *J. Phys. Chem.* 70:2869–2872.

Huie, R. E., and S. Padmaja. 1993. The reaction of NO with superoxide. *Free Rad. Res. Comm.* 18:195–199.

Imlay, J. A., and I. Fridovich. 1991. Assay of metabolic superoxide production in *Escherichia coli. J. Biol. Chem.* 266:6957–6965.

Iyengar, R., D. J. Stuehr, and M. A. Marletta. 1987. Macrophage synthesis of nitrite, nitrate, and N-nitrosamines: precursors and role of the respiratory burst. *Proc. Natl. Acad. Sci. USA.* 84:6369–6373.

Koppenol, W. H., J. J. Moreno, W. A. Pryor, H. Ischiropoulos, and J. S. Beckman. 1992. Peroxynitrite: a cloaked oxidant from superoxide and nitric oxide. *Chem. Res. Toxicol.* 5:834–842.

Lancaster, J. R., Jr. 1994. Simulation of the diffusion and reaction of endogenously produced nitric oxide. *Proc. Natl. Acad. Sci. USA.* 91: 8137–8141.

Lancaster, J. R., Jr. 1996. Diffusion of free nitric oxide. *Methods Enzymol.* 268:31–50.

Lewis, R. S., and W. M. Deen. 1994. Kinetics of the reaction of nitric oxide with oxygen in aqueous solutions. *Chem. Res. Toxicol.* 7:568–574.

Lewis, R. S., S. Tamir, S. R. Tannenbaum, and W. M. Deen. 1995a. Kinetic analysis of the fate of nitric oxide synthesized by macrophages in vitro. *J. Biol. Chem.* 270:29350–29355.

Lewis, R. S., S. R. Tannenbaum, and W. M. Deen. 1995b. Kinetics of N-nitrosation in oxygenated nitric oxide solutions at physiological pH: role of nitrous anhydride and effects of phosphate and chloride. *J. Am. Chem. Soc.* 117:3933–3939.

Licht, W. R., S. R. Tannenbaum, and W. M. Deen. 1988. Use of ascorbic acid to inhibit nitrosation: kinetic and mass transfer considerations for an in vitro system. *Carcinogenesis.* 9:365–372.

Lymar, S. V., and J. K. Hurst. 1995. Rapid reaction between peroxynitrite ion and carbon dioxide: implications for biological activity. *J. Am. Chem. Soc.* 117:8867–8868.

Marletta, M. A. 1993. Nitric oxide synthase structure and mechanism. *J. Biol. Chem.* 268:12231–12234.

Miles, A. M., D. S. Bohle, P. A. Glassbrenner, B. Hansert, D. A. Wink, and M. B. Grisham. 1996. Modulation of superoxide-dependent oxidation and hydroxylation reactions by nitric oxide. *J. Biol. Chem.* 271:40–47.

Moncada, S., R. M. J. Palmer, and E. A. Higgs. 1991. Nitric oxide: physiology, pathophysiology, and pharmacology. *Pharmacol. Rev.* 43: 109–142.

Nagata, S. 1975. Mixing Principles and Applications. Kodansha, Tokyo. 25–39.

Newman, J. S. 1973. Electrochemical Systems. Prentice-Hall, Englewood Cliffs, NJ. 230.

Pfeiffer, S., A. C. F. Gorren, K. Schmidt, E. R. Werner, B. Hansert, D. S. Bohle, and B. Mayer. 1997. Metabolic fate of peroxynitrite in aqueous solution. *J. Biol. Chem.* 272:3465–3470.

Press, W. H., S. A. Teukolsky, W. T. Vetterling, and B. P. Flannery. 1972. Numerical Recipes in Fortran. Cambridge University Press, Cambridge. 372–385, 745–777.

Schwartz, S. E. 1983. Trace atmospheric constituents: properties, transformations, and fates. *In* Advances in Environmental Science and Technology J. O. Nriagu, editor. Wiley, New York. 1–115.

Tamir, S., and S. R. Tannenbaum. 1996. The role of nitric oxide (NO) in the carcinogenic process. *Biochim. Biophys. Acta.* 1288:F31–F36.

Uppu, R. M., G. L. Squadrito, and W. A. Pryor. 1996. Acceleration of peroxynitrite oxidations by carbon dioxide. *Arch. Biochem. Biophys.* 327:335–343.

Wise, D. L., and G. Houghton. 1968. Diffusion coefficients of neon, krypton, xenon, carbon monoxide, and nitric oxide in water at 10–60°C. *Chem. Eng. Sci.* 23:1211–1216.

Wood, J., and J. Garthwaite. 1994. Models of the diffusional spread of nitric oxide: implications for neural nitric oxide signaling and its pharmacological properties. *Neuropharmacology.* 11:1235–1244.